Organic Electronics 43 (2017) 148–155

Contents lists available at ScienceDirect

Organic Electronics

journal homepage: www.elsevier.com/locate/orgel

Thermal annealing effect on organic semiconducting polymer laser with an external holographic grating feedback layer

Guiyang Zhang [a, b], Qidong Wang [a], Yonggang Liu [a], Ji Ma [c, **], Zenghui Peng [a], Lishuang Yao [a], Dayu Li [a], Chengliang Yang [a], Quanquan Mu [a], Zhaoliang Cao [a], Li Xuan [a, *]

[a] State Key Laboratory of Applied Optics, Changchun Institute of Optics, Fine Mechanics and Physics, Chinese Academy of Sciences, Changchun, 130033, China
[b] University of Chinese Academy of Sciences, Beijing, 100049, China
[c] Liquid Crystal Institute, Kent State University, OH, 44240, USA

ARTICLE INFO

Article history:
Received 21 October 2016
Received in revised form
7 January 2017
Accepted 7 January 2017
Available online 8 January 2017

Keywords:
Annealing effect
Organic semiconducting distributed feedback laser
Amplified spontaneous emission
Energy conversion efficiency

ABSTRACT

Thermal annealing effect on an organic distributed feedback (DFB) laser excited from a semiconducting polymer gain layer, poly(2-methoxy-5-(2'-ethyl-hexyloxy)-p-phenyl-envinylene) (MEH-PPV), is reported. The morphology, absorption and photoluminescence (PL) spectral characteristics of the MEH-PPV film annealed at different temperatures were analyzed. The amplified spontaneous emission (ASE), the optical gain and loss coefficients were also investigated. The organic lasing behaviors including threshold, energy conversion efficiency and polarization state in a DFB laser device were studied. The results show that the optical properties of the organic semiconducting laser can be enhanced by thermal annealing effect. The single mode laser emission at 622.4 nm with lower lasing threshold 0.2 μJ/pulse and higher energy conversion efficiency 6.71% was achieved with thermal annealing at 120 °C. The thermal annealing treatment decreases laser threshold and increases laser energy conversion efficiency dramatically, which shows the potential in ultra-low cost organic semiconducting polymer DFB lasers.

1. Introduction

Organic semiconductor lasers (OSLs) have drawn much scientific attention recently because of their potential for various applications, such as spectral analysis, optical communications, chemical sensors and display systems [1–4]. Since the report of laser action from conducting polymer solution in 1992, organic semiconducting materials become a new class of material that combines optical and electronic properties of semiconductors, showing advantages like low cost, simple process and better flexibility [5,6]. Organic semiconducting polymer materials exhibit strong absorption, wide fluorescence bands, high fluorescence quantum efficiency and large Stokes shift [7–10]. Through proper modifying molecular structures, especially by adding alkoxy substitutions to polymer side chains or changing molecular geometric size in synthetic process, polymer properties and processing can be modulated [11]. The polymer properties are determined by molecular structure, conformation and molecular size [12]. Therefore we can design organic semiconducting materials with preferable photoelectric properties to fulfill different demands in practice. On the other hand, adding flexible side chain groups promotes the solubility of polymers in ordinary aromatic and non-aromatic solvents [13]. Thus, these organic semiconducting materials can be solution-processed to form thin films with different geometrical shapes at room temperature by spin-coating, drop-cast, inkjet-print or other methods [14]. All of these excellent features make semiconducting polymer materials ideal for photoelectric and opto-optical devices applications.

Researchers have done a great deal of work on organic polymer films to explore their properties in the past decades. They mainly focused on studying the relationship between molecular weight and chain orientation in the films, aggregation behaviors, solvent effect, thickness-dependent optical properties, refractive index distribution and energy transfer between finite segments in the polymer films [15–19]. Besides these studies, they also investigated the annealing effect on the polymer films. Attention was paid to explore the current-voltage-luminance (I-V-L) behavior and power conversion efficiency because the thermal annealing treatment can

* Corresponding author.
** Corresponding author.
E-mail addresses: jma2@kent.edu (J. Ma), xuanli@ciomp.ac.cn (L. Xuan).

http://dx.doi.org/10.1016/j.orgel.2017.01.011
1566-1199/

change the spatial uniformity, charge carrier mobility, thermal stability of the polymer film and capability to endure the Joule heat generated during the operation [20–24]. Since only organic semiconducting polymer films have been studied for amplified spontaneous emission (ASE) by far, in this work we contribute thermal annealing effect on the semiconducting polymer films for organic distributed feedback (DFB) laser applications.

In this paper, the thermal annealing effect on the semiconducting polymer Poly (2-methoxy-5-(2'-ethyl-hexyloxy)-p-phenyl-en-evinylene) (MEH-PPV) layer was performed in a DFB laser device with a periodic holographic polymer dispersed liquid crystal (HPDLC) grating layer as the external light feedback layer [25]. The film morphologies, spectroscopic characteristics and organic DFB laser behaviors were investigated. Theoretically and experimentally, we proved the thermal annealed MEH-PPV film showed better performance on laser threshold and energy conversion efficiency for DFB lasers.

2. Experiments

2.1. Thin film preparation

The organic semiconducting MEH-PPV (M_n = 43324, M_w = 242954, as determined by GPC) was purchased from Xi'an *P*-OLED Material Corporation and used as received. The solutions with a certain concentration (0.8 wt%) of MEH-PPV were prepared in chlorobenzene (CB) solvent. Then the solution was spin-coated on the surface of a cleaned glass substrate for 30 s, resulting in a homogeneous thin film. The spin-cast MEH-PPV layer thickness was measured by a Dektak Profilometer and the parameters of each sample were shown in Table 1. The glass transition temperature (T_g) of the MEH-PPV we used here was in the vicinity of 65 °C (determined by DSC), which is consistent with previous reports [24,26]. After spin-coating, the organic polymer film was heated in a vacuum oven at a 2 °C/min heating rate from room temperature to the desired annealing temperature and remained at the annealing temperature for 1 h, then followed by slowly cooling to room temperature.

2.2. HPDLC grating fabrication

The materials adopted in the mixture for HPDLC were LC TEB30A (n_o = 1.522, n_e = 1.692, Slichem, 28 wt%), N-vinylpyrrolidone (NVP, Sigma-Aldrich, 10 wt%) as a solvent and a chain extender, photo-initiator Rose Bengal (RB, Sigma-Aldrich, 0.5 wt%), coinitiator N-phenylglycine (NPG, Sigma-Aldrich, 1.5 wt%), difunctional acrylate monomer phthalicdiglycoldiacrylate (PDDA, Sigma-Aldrich, 30 wt%) and penta-functional acrylate monomer dipentaerythritol hydroxyl pentaacrylate (DPHPA, Sigma-Aldrich, 30 wt %). The mixture was stirred in dark for 24 h and injected into the empty cell. The cell was pre-fabricated by combining the MEH-PPV film coated glass substrate with the other pre-cleaned glass substrate and the cell gap was controlled at 6 μm by Mylar spacers. After being injected into the cell by capillary effect at 25 °C, the cell underwent holographic photo-curing by two coherent s-polarized laser beams from a 532 nm Nd:YAG laser to form the HPDLC structure by photo-polymerization induced phase separation [27]. The light intensity of each recording beam was 2.5 mW/cm^2 and the exposure time was 3 min. The fabricating setup and the morphology of HPDLC grating are illustrated in Fig. 1. The core MEH-PPV layer along with the top HPDLC grating layer and the bottom glass layer forms an asymmetric slab waveguide configuration. The grating area was 2 cm by 2 cm. The HPDLC grating period (Λ) can be controlled according to

$$\Lambda = \frac{\lambda_{532}}{2\sin\left(\theta/2\right)} \quad (1)$$

and θ was the intersection angle between the two coherent recording beams. The period of the grating was 586 nm to obtain light feedback through the third Bragg order for MEH-PPV gain layer.

2.3. Diffraction efficiency measurement

To make sure that all the HPDLC gratings have similar morphologies, the diffraction efficiency of each sample was measured by a He–Ne laser (circular polarization, 632.8 nm) at the incident Bragg angle onto the sample and the first order diffracted beam was measured by Detector 2. The diffraction efficiency is defined as the first order diffracted light intensity ($I_{1\chi}$) plus the zeroth order light intensity (I_0) and then divided by $I_{1\chi}$, here χ is the s or p polarization state obtained by rotating the polarizer in the light path. The diffraction efficiency values were also shown in Table 1.

2.4. Optical properties measurement of MEH-PPV films

The absorption and photoluminescence (PL) spectra of MEH-PPV layers were measured by UV–Vis spectrophotometer (Shimadzu UV-3101; Shimadzu Corp., Japan) and fluorescence spectrophotometer (Hitachi F-7000; Hitachi, Ltd., Japan), respectively. The absolute value of the photoluminescence quantum yield (PLQY) of MEH-PPV films were measured by a fluorescence spectrometer (FL920; Edinburgh Instruments, China).

2.5. Optical pumping

For optical pumping, a Q-switched Nd:YAG pulsed laser operating at 532 nm (repetition rate: 2 Hz and pulse duration: 8.6 ns) was used for our samples. The intensity of the pump light was controlled using calibrated neutral density filters. A cylindrical lens with focal length 20 cm and an adjustable slit were used to shape the pump beam into a narrow stripe of dimension 4 mm by 0.1 mm,

Table 1
Parameters of different samples in the experiment.

Sample ID[a]	Annealing temperature (°C)	Thickness of MEH-PPV (nm)		η_s (%)	η_p (%)
		Before annealing	After annealing		
a1	25	85	85	2.8	94
a2	50	85	85	2.6	93.4
a3	80	85	81.6	2.2	93.2
a4	100	85	80.5	2.8	96.3
a5	120	85	80	2.2	93.3
a6	150	85	79.8	2.1	95

[a] All the films were annealed in vacuum oven and the grating periods were 586 nm. Each of the film thickness was measured at five times to get a mean value.

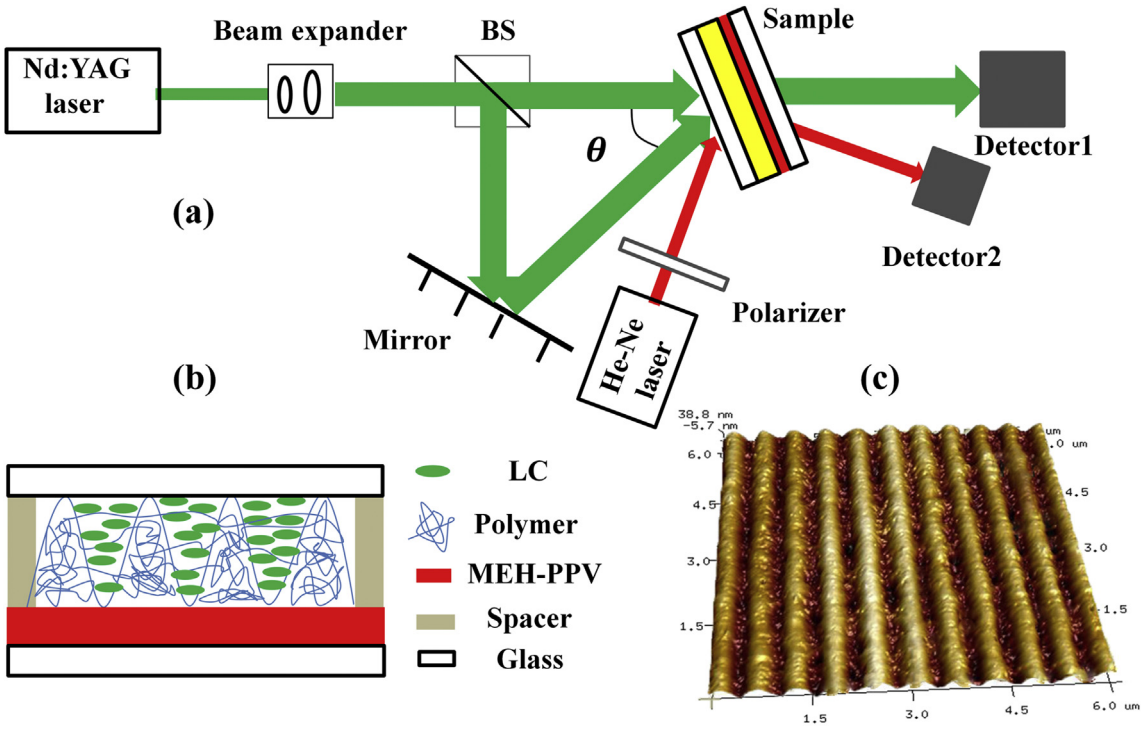

Fig. 1. (a) Writing and diffraction efficiency measuring setup for HPDLC grating, (b) schematic device structure and (c) three dimensional AFM image of the HPDLC.

thus creating a stripe shaped gain region. The excitation light was collected from the edge of the sample with an optical fiber spectrometer and a CCD energy meter was used to measure the output laser energy. The schematic setup of the lasing experiment is shown in Fig. 2.

3. Results and discussion

3.1. MEH-PPV surface morphology properties

The surface morphology properties of the MEH-PPV films were investigated by high performance atomic force microscopy (AFM). Fig. 3 shows three dimensional topographic images of the MEH-PPV film for 2 μm by 2 μm scan area. Compared with the film drying at 25 °C, the surface morphology changed negligibly when MEH-PPV film was annealed at 50 °C, for the root mean square (RMS) value, which represents the degree of the surface roughness, varied from 2.74 nm to 2.72 nm. When MEH-PPV films were annealed at 80, 100, 120 and 150 (°C), the RMS values were 1.52, 1.25, 0.83 and 0.56 (nm), respectively. The degree of the surface roughness was decreased with thermal annealing temperature.

A smoother surface was observed with the annealing temperature increasing because the chain movement was enhanced at the temperature above the T_g [28]. Thermal treatment temperature below and above the T_g of MEH-PPV would generate distinct difference. The drying treatment at 25 °C, 50 °C below the T_g of the MEH-PPV film were purely used to move away the CB solvent residual after film casting, but the annealing temperature above the T_g was altering the morphology of semiconducting MEH-PPV film and we believe that it would influence the optical properties of organic gain films [29].

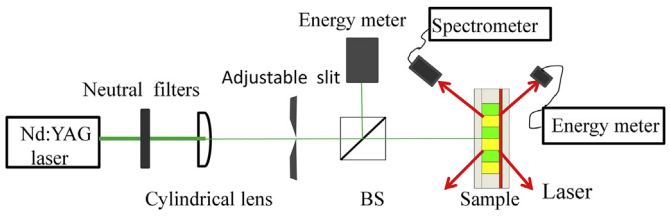

Fig. 2. Optical setup for pumping the organic DFB sample and collecting the output emission.

3.2. Optical properties of the MEH-PPV films

The Absorption, PL and ASE spectra of the annealing treatment organic MEH-PPV solid films were demonstrated in Fig. 4. The spectra of the organic films showed obvious difference with different annealing temperatures. The absorption peak had red shift from 500 nm to 509 nm and the PL peak shifted from 590 nm to 604 nm, with the annealing temperature range from 25 °C to 150 °C, as shown in Fig. 4(a). With the increase of annealing temperature, the polymer chains can move more freely, which is helpful to the change of the twist angle of the ring through the chains rearrangement to coplanarization, thus the π-delocalization is enhanced and the $\pi \rightarrow \pi^*$ energy gap is decreased, making the absorption/PL spectra red shift [23,24]. The broad spectral overlap between the absorption spectra and the PL spectra from 520 nm to 600 nm suggests that laser can not be obtained below 600 nm due to self-absorption effect.

Moreover, we noticed the dramatic change on PL intensities with annealing temperature increasing, but the absorption intensities were similar from different films. We consider that two reasons can explain the phenomenon. The first reason is that each MEH-PPV film is formed with the same amount of MEH-PPV solution, so the amount of luminous chromospheres are equal for all the films, thus the absorption intensity of organic films are coincide with each other. The other reason is attributing to annealing treatment at proper temperature above the T_g, thereby the polymer

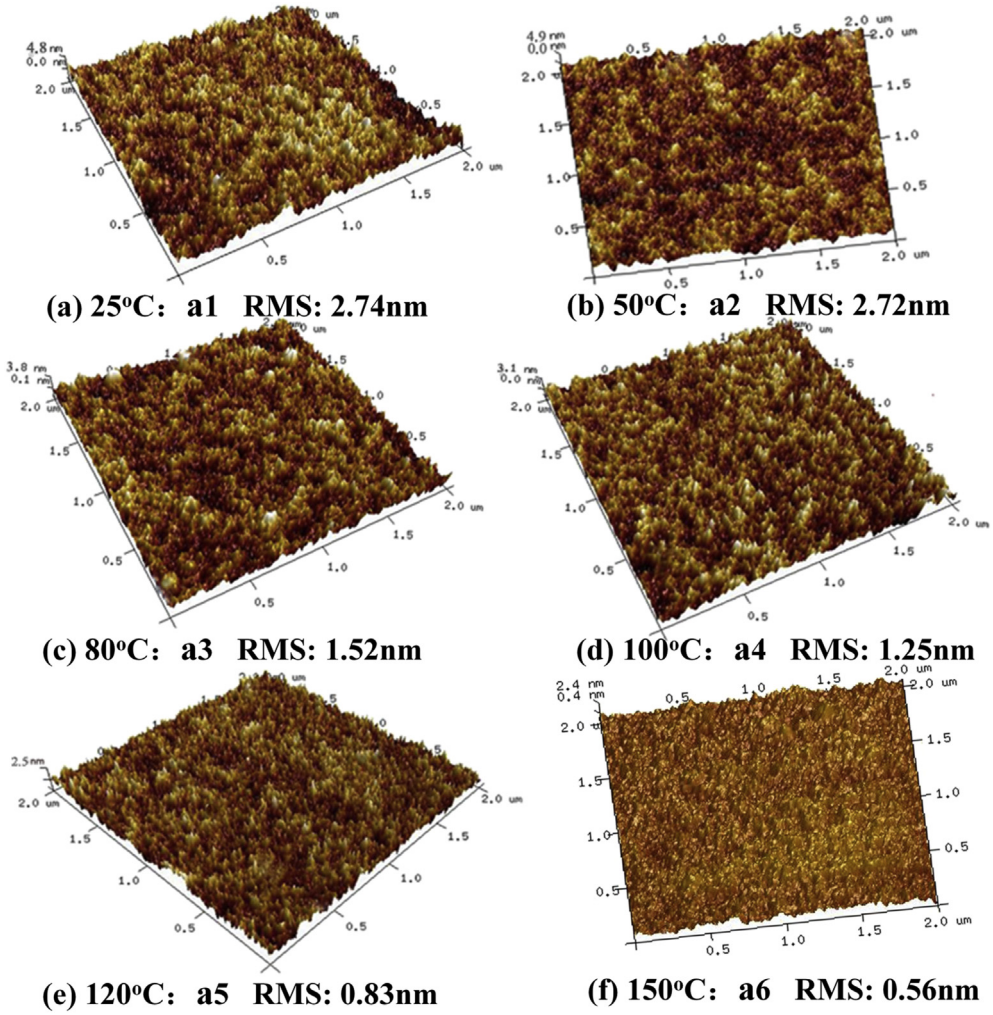

Fig. 3. AFM images of the MEH-PPV surface after drying at (a) 25 °C and annealing at (b) 50 °C, (c) 80 °C, (d) 100 °C, (e) 120 °C and (f) 150 °C.

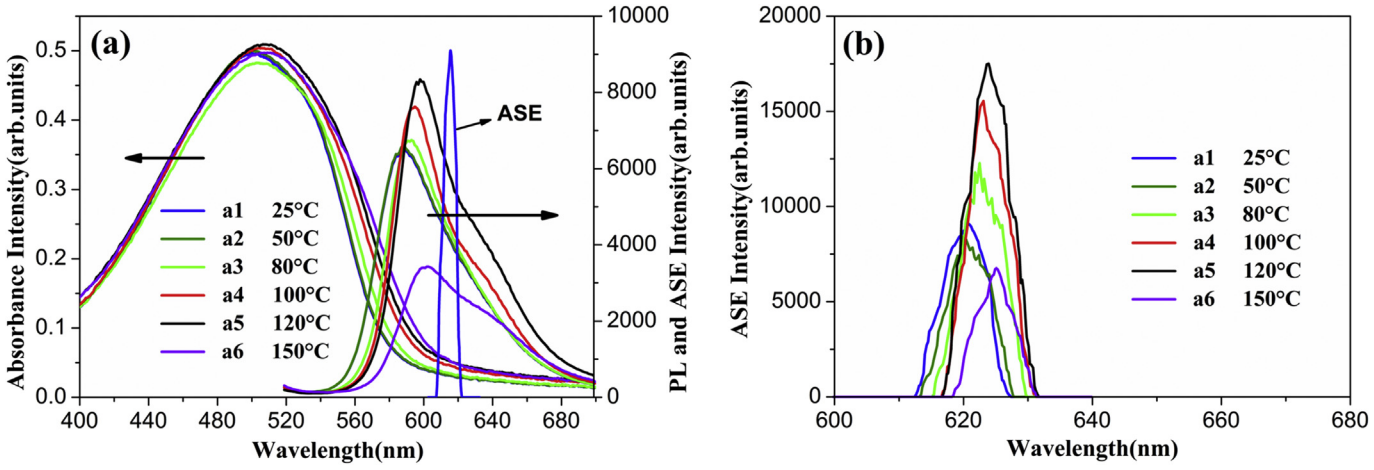

Fig. 4. (a) ASE spectra drying at 25 °C, absorption and PL spectra and (b) ASE spectra from MEH-PPV films annealed at different temperatures.

chains can move more freely, enhancing the packing of the polymer film and eliminating some of the free volume or pores remaining after the evaporation of the solvent. This makes the surface of films smooth and reduces the scattering loss from MEH-PPV films, which can be forecast from the morphologies shown in Fig. 3. While too high annealing treatment induces nanoscale modulation, excimers or other non-radiation species, it would reduce the luminescence quantum yield [30,31]. So the sudden decline of PL intensity with 150 °C annealing temperature occurred.

We also measured the ASE spectra from the edge of sample with

polymer dispersed liquid crystal (PDLC) layer, which the prepolymer mixture is exposed to a single laser beam with an intensity of 20 mW/cm^2 [32], under 532 nm pulse optical pumping, as shown in Fig. 4(b). ASE is an amplified spontaneous emission and located at the maximum of the gain spectra which can be seen as a signal of the lasing performance of the gain medium [33]. The ASE peak of gain layer drying under 25 °C located at 620 nm with a full width at half maximum (FWHM) of nearly 8 nm while the ASE peaks of films annealing at other temperature red shift from 620 nm to 625 nm slightly.

Fig. 5 shows the dependence of the spectrally integrated PL intensity emitted from the edge of the film on the pump intensity annealed at different temperatures. The inset in Fig. 5 shows the corresponding ASE threshold, which can be determined from the abrupt rise in the output intensity. We compared the ASE threshold for **a3** (annealed at 80 °C) with other report [34]. The threshold value 12 μJ/cm^2 for the CB-cast MEH-PPV film annealed at 80 °C was obtained in the report and the result was smaller than that in our experiment. The increased ASE threshold was generated from the scattering loss in PDLC layer, as ~100 nm scale liquid crystal droplets formed in the structure [32].

The absolute values of the photoluminescence quantum yield (PLQY) of MEH-PPV films annealed at different temperatures were measured by an integrating sphere and the measurement error was 10%. As illustrated in Fig. 6, the PLQY values increased to 32% with the annealing temperature increased to 120 °C, then followed by an abrupt decrease with 150 °C annealing treatment. The PLQY value 23% was achieved for sample dry at room temperature which is comparable with other reports [16,35–37].

Fig. 7(a) shows the output intensity at 622 nm as a function of pump stripe length for MEH-PPV films annealed at different temperatures at 4 kW/cm^2. The output intensity should fulfill the following expression [38]:

$$I(\lambda) = \frac{A(\lambda)I_P}{g(\lambda)}\left(e^{g(\lambda)l} - 1\right) \quad (2)$$

Where A is a constant related to the cross section for spontaneous emission, I_p is the pump intensity, g is the net gain coefficient, and l is the length of the pumped stripe. The solid lines are fits to the exponential subset of the corresponding data using Eq. (2) with the parameters listed in Table 2.

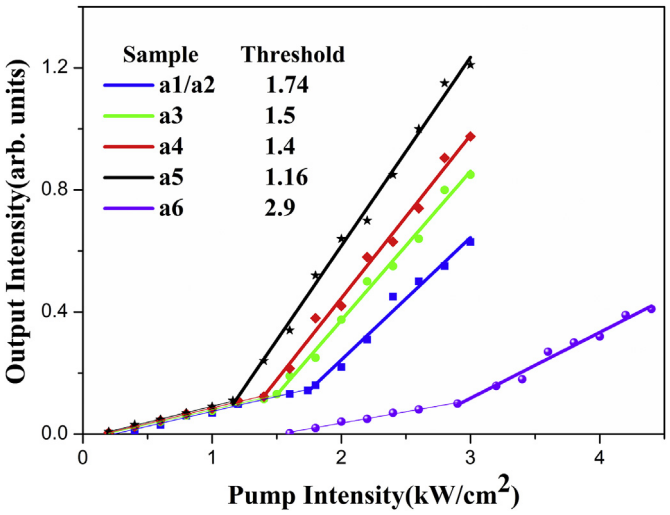

Fig. 5. The relationship between the total emission intensity integrated over all wavelengths and pump intensity. The pump stripe was 4 mm × 0.1 mm.

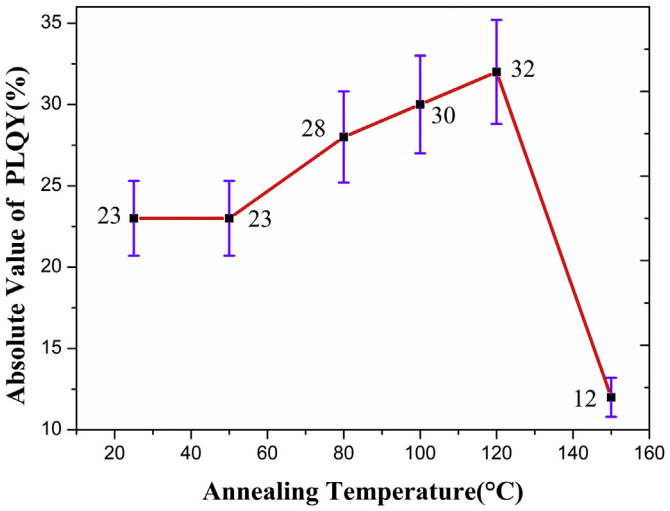

Fig. 6. Absolute values of the PLQY of MEH-PPV films annealed at different temperatures.

To further characterize the effective waveguide losses of conjugated polymers, we performed the experiment that kept the length of the pump stripe constant and moved the pump stripe away from the edge of samples. As shown in Fig. 7(b), the emitted intensity from the end of the pump stripe is constant, the emitted intensity from the edge of samples should decrease according to

$$I(\lambda) = I_0(\lambda)\exp[-\alpha(\lambda)x] \quad (3)$$

where x is the length of the unpumped region between the end of the pump stripe and.

the edge of the sample, $\alpha(\lambda)$ is the overall loss coefficient, which includes both absorption and scattering loss, and $I_0(\lambda)$ is the spontaneous emission intensity at the end of the pump stripe. By curve fitting these data to Eq. (3), we measured the loss coefficients were 14, 11, 10, 8.5 and 17.6 (cm^{-1}) for sample **a1**-**a6**, respectively. We noticed that the sample **a6** annealed at 150 °C with the minimum film surface roughness (RMS: 0.56 nm) exhibited the maximal loss coefficient 17.6 cm^{-1}.

After measuring the absolute values of PLQY, the net gain coefficient and the loss coefficient of MEH-PPV films annealed at different temperatures, we found that the net gain coefficient changed with the PLQY value and the loss coefficient. The higher the PLQY value and the lower the loss coefficient, the greater the net gain coefficient is. So the maximal net gain coefficient achieved at 120 °C annealed treatment with the highest PLQY value 32% and the lowest loss coefficient 8.5 cm^{-1}. This result is in good agreement with previous theory [39] and we can see that the laser performance would follow the net gain coefficient.

3.3. Laser performance

When optically pumped, the laser emission occurred from our device. Fig. 8 shows the emission lasing spectra and corresponding lasing intensity depending on pump intensity of different samples. The lasing peaks located at 622.4 nm–625 nm at a pumping energy density of 1.60 μJ/pulse for the samples in Fig. 8(a). The different lasing peak positions were generated from the different MEH-PPV gain film thickness and the thicker film would lead to the longer lasing wavelength [40]. Besides, the energy conversion efficiency of all the samples was measured with 45° polarized pump light incident normal to the surface of glass substrate. Fig. 8(b) shows the

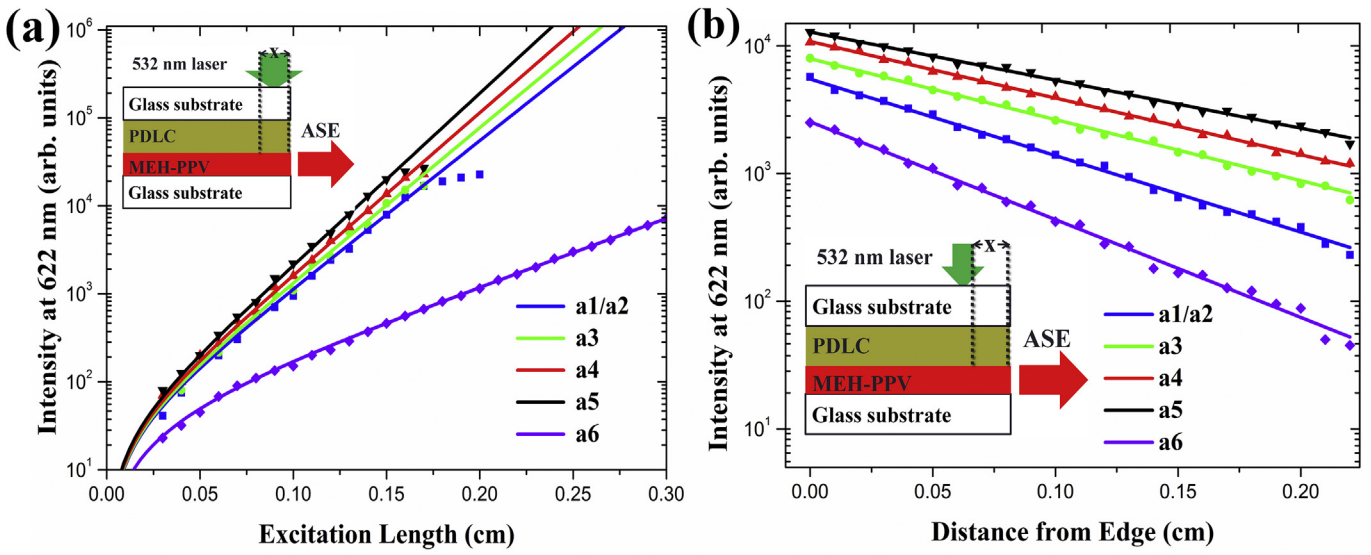

Fig. 7. Dependence of the emission intensity at 622 nm on the (a) excitation length at the indicated pump intensity and (b) distance x between the sample edge and the excitation stripe.

Table 2
Parameters obtained from fits of Eq. (2) to the data in Fig. 7(a).

Sample ID*	Pump intensity (kW/cm^2)	AI_p (arb. units)	g (cm^{-1})
a1/a2	4	928	38.6
a3	4	950	41
a4	4	1000	42.5
a5	4	1050	45
a6	4	610	18

5.8% for sample **a1** and the highest value of 6.71% is obtained for sample **a5**, while it is the lowest 2.58% for sample **a6**. Therefore, the laser threshold is 0.33 μJ/pulse for sample **a1**, the lowest value 0.20 μJ/pulse for sample **a5** and the highest value 0.90 μJ/pulse for sample **a6**. The performance of laser emitted from **a1** was worse than that in previous report using the same laser feedback structure [41]. This was attributed to the optical gain coefficient in the report was higher than that in our experiment for the different MEH-PPV

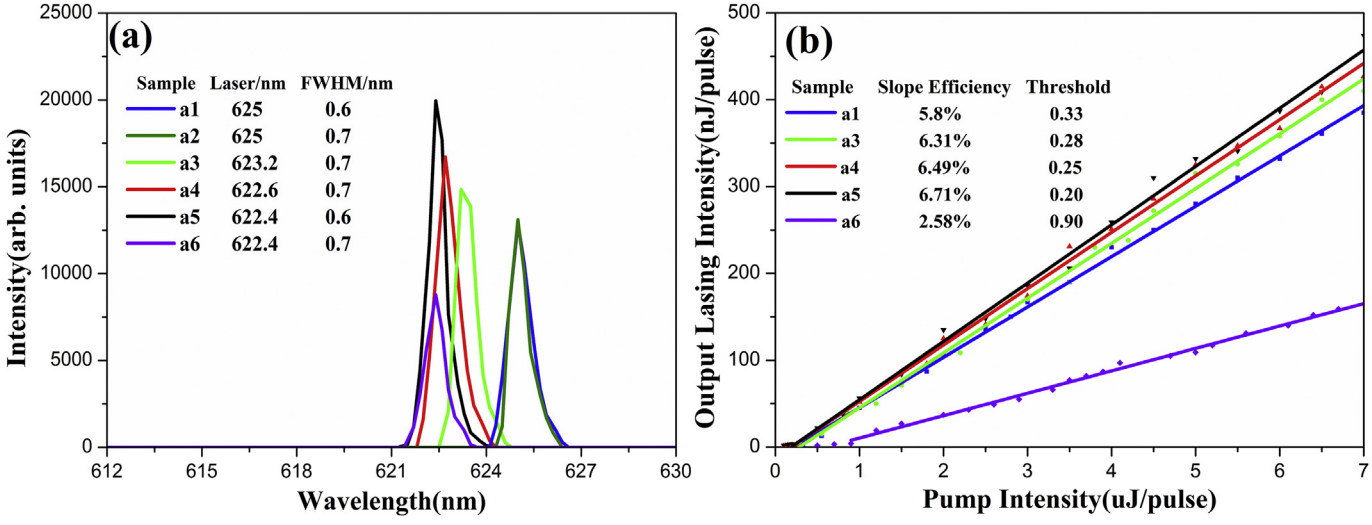

Fig. 8. (a) Output lasing spectra and (b) the relationship between lasing intensity and pump intensity of samples annealed at different temperatures.

dependence of output lasing energy on the pump energy for samples except **a2** as it is the same as **a1**. The solid squares are experimental data and the five curves are linear fit to the correlative data. The intersection between these linear lines with the pump energy axis provide laser thresholds and their slopes give energy conversion efficiencies.

The inset in Fig. 8(b) illustrates the corresponding slop efficiency and lasing threshold for each sample. The output slope efficiency is

molecular weight, different solvent and different concentration used in the experiment [42]. Besides, we also compared the result with other reports using different laser feedback structure. A second-order laser was obtained from the two-dimensional (2D) square array grating (grating period: 409 nm) feedback structure [43]. The 2D grating structure provided 2D feedback effect and the smaller grating periods further enhanced the laser feedback, thus the lasing threshold was decreased and the slope efficiency was

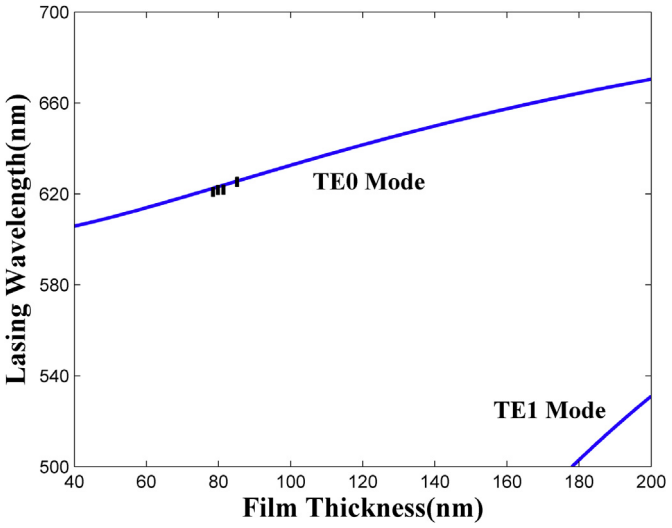

Fig. 9. Theoretical lasing wavelength as a function of MEH-PPV film thickness for zeroth order and first order TE modes.

improved. However, a third-order laser emitted from one-dimensional (1D) nanoimprint lithography MEH-PPV grating (grating period: 600 nm) with higher lasing threshold was achieved [44]. This result was attributed to the thick film thickness (240 nm), which was too thick to impede the energy feedback between the interfaces.

Considering that the organic laser wavelength λ follows the Bragg equation and asymmetric TE waveguide equation:

$$m\lambda = 2n_{eff}\Lambda \tag{4}$$

$$\frac{2\pi h}{\lambda}\sqrt{n_{MEH}^2 - n_{eff}^2} = M\pi + \tan^{-1}\sqrt{\frac{n_{eff}^2 - n_{glass}^2}{n_{MEH}^2 - n_{eff}^2}} + \tan^{-1}\sqrt{\frac{n_{eff}^2 - n_{grating}^2}{n_{MEH}^2 - n_{eff}^2}} \tag{5}$$

where ∧ is the grating period, m is the Bragg order, which was selected as 3 in the experiment. h is the film thickness, M is an integer that accounts for the mode order,n_{eff} is the effective refractive index of the laser mode, n_{MEH}, n_{glass} and $n_{grating}$ are 1.90,1.516 and 1.54, respectively [45–47]. The refractive index of MEH-PPV film is approximately 1.90 for the TE mode and 1.52 for the TM mode, thus TM mode would leak out from the structure. As shown in Fig. 9, all the film thickness is thinner than 178 nm in the experiment, the output laser only contains TE0 mode.

4. Conclusions

In conclusion, we have demonstrated the effects of annealing treatment on MEH-PPV film in the organic DFB laser based on an external HPDLC feedback structure. We find that the MEH-PPV film with thermal annealing treatment at 120 °C exhibits the highest energy conversion efficiency 6.71% and the lowest lasing threshold 0.2 μJ/pulse. Taking optical properties and laser performance of organic films into consideration, we conclude that thermal annealing treatment at proper temperature can enhance the organic DFB laser performance by optimizing film morphology for waveguide structure and increasing PL intensity. This work will give more understanding of thermal annealing effect on organic DFB laser application and make contribution to the development of organic semiconducting polymer lasers.

Acknowledgements

The authors would like to thank the National Natural Science Foundation of China (Grant Nos. 61475152, 61377032, 11604327, 61405194) for the support.

References

[1] T. Woggon, S. Klinkhammer, U. Lemmer, Compact spectroscopy system based on tunable organic semiconductor lasers, Appl. Phys. B 99 (2010) 47–51.
[2] J. Clark, G. Lanzani, Organic photonics for communications, Nat. Phot. 4 (2010) 438–446.
[3] D.T. McQu bade, A.E. Pullen, T.M. Swager, Conjugated polymer-based chemical sensors, Chem. Rev. 100 (2000) 2537–2574.
[4] K. Seung Hwan, P. Heng, L. Daeho, P.G. Costas, K.P. Hee, Nanoparticle selective laser processing for a flexible display fabrication, Jpn, J. Appl. Phys. 49 (2010) 05EC03.
[5] D. Moses, High quantum efficiency luminescence from a conducting polymer in solution: a novel polymer laser dye, Appl. Phys. Lett. 60 (1992) 3215–3216.
[6] B.J. Schwartz, Conjugated polymers as molecular materials: how chain conformation and film morphology influence energy transfer and interchain interactions, Annu. Rev. Phys. Chem. 54 (2003) 141–172.
[7] Y. Li, Molecular design of photovoltaic materials for polymer solar cells: toward suitable electronic energy levels and broad absorption, Acc. Chem. Res. 45 (2012) 723–733.
[8] C. Xiang, W. Koo, F. So, H. Sasabe, J. Kido, A systematic study on efficiency enhancements in phosphorescent green, red and blue microcavity organic light emitting devices, Light Sci. Appl. 2 (2013) e74.
[9] M. Fröbel, T. Schwab, M. Kliem, S. Hofmann, K. Leo, M.C. Gather, Get it white: color-tunable AC/DC OLEDs, Light Sci. Appl. 4 (2015) e247.
[10] D. Zhang, L. Duan, Y. Zhang, M. Cai, D. Zhang, Y. Qiu, Highly efficient hybrid warm white organic light-emitting diodes using a blue thermally activated delayed fluorescence emitter: exploiting the external heavy-atom effect, Light Sci. Appl. 4 (2015) e232.
[11] Z. George, R. Kroon, R. Gehlhaar, G. Gbabode, A. Lundin, S. Hellström, C. Müller, Y. Geerts, P. Heremans, M.R. Andersson, The influence of alkoxy substitutions on the properties of diketopyrrolopyrrole-phenyl copolymers for solar cells, Materials 6 (2013) 3022–3034.
[12] D. Wang, Y. Yuan, Y. Mardiyati, C. Bubeck, K. Koynov, From single chains to aggregates, how conjugated polymers behave in dilute solutions, Macromolecules 46 (2013) 6217–6224.
[13] C.-C. Chang, C.-L. Pai, W.-C. Chen, S.A. Jenekhe, Spin coating of conjugated polymers for electronic and optoelectronic applications, Thin solid films 479 (2005) 254–260.
[14] L.-Y. Wong, R.-Q. Png, F.S. Silva, L.-L. Chua, D.M. Repaka, X.-Y. Gao, L. Ke, S.-J. Chua, A.T. Wee, P.K. Ho, Interplay of processing, morphological order, and charge-carrier mobility in polythiophene thin films deposited by different methods: comparison of spin-cast, drop-cast, and inkjet-printed films, Langmuir 26 (2010) 15494–15507.
[15] K. Koynov, A. Bahtiar, T. Ahn, C. Bubeck, H.-H. Hörhold, Molecular weight dependence of birefringence of thin films of the conjugated polymer poly [2-methoxy-5-(2′-ethyl-hexyloxy)-1, 4-phenylenevinylene], Appl. Phys. Lett. 84 (2004) 3792–3794.
[16] T.-Q. Nguyen, I.B. Martini, J. Liu, B.J. Schwartz, Controlling interchain interactions in conjugated polymers: the effects of chain morphology on exciton-exciton annihilation and aggregation in MEH-PPV films, J. Phys. Chem. B 104 (2000) 237–255.
[17] R. Traiphol, R. Potai, N. Charoenthai, T. Srikhirin, T. Kerdcharoen, T. Osotchan, Effects of chain conformation and chain length on degree of aggregation in assembled particles of conjugated polymer in solvents–nonsolvent: a spectroscopic study, J. Polym. Sci. Part B Polym. Phys. 48 (2010) 894–904.
[18] V. Cimrova, D. Neher, Microcavity effects in single-layer light-emitting devices based on poly (p-phenylene vinylene), J. Appl. Phys. 79 (1996) 3299–3306.
[19] T.-Q. Nguyen, J. Wu, V. Doan, B.J. Schwartz, S.H. Tolbert, Control of energy transfer in oriented conjugated polymer-mesoporous silica composites, Science 288 (2000) 652–656.
[20] A. Reshak, M. Shahimin, N. Juhari, S. Suppiah, Electrical behaviour of MEH-PPV based diode and transistor, Prog. Biophys. Mol. Biol. 113 (2013) 289–294.
[21] H. Jin, Y. Hou, X. Meng, Y. Li, Q. Shi, F. Teng, Enhanced photovoltaic properties of polymer–fullerene bulk heterojunction solar cells by thermal annealing, Solid State Commun. 142 (2007) 181–184.
[22] T.-Q. Nguyen, B.J. Schwartz, R.D. Schaller, J.C. Johnson, L.F. Lee, L.H. Haber, R.J. Saykally, Near-field scanning optical microscopy (NSOM) studies of the relationship between interchain interactions, morphology, photodamage, and energy transport in conjugated polymer films, J. Chem. Phys. B 105 (2001) 5153–5160.
[23] T. J.Savenije, J.E. Kroeze, X. Yang, J. Loos, The effect of thermal treatment on the morphology and charge carrier dynamics in a polythiophene-fullerene

bulk heterojunction, Adv. Funct. Mater 15 (2005) 1260–1266.
[24] T.-W. Lee, O.O. Park, The effect of different heat treatments on the luminescence efficiency of polymer light-emitting diodes, Adv. Mater 12 (2000) 801–804.
[25] Z. Diao, L. Kong, L. Xuan, J. Ma, Electrical control of the distributed feedback organic semiconductor laser based on holographic polymer dispersed liquid crystal grating, Org. Electron 27 (2015) 101–106.
[26] Y. Liu, M.S. Liu, X.-C. Li, A.K. Jen, Synthesis and characterization of a novel light-emitting polymer containing highly efficient hole-transporting aromatic diamine, Chem. Mater 10 (1998) 3301–3304.
[27] L. Liu, L. Xuan, G. Zhang, M. Liu, L. Hu, Y. Liu, J. Ma, Enhancement of pump efficiency for an organic distributed feedback laser based on a holographic polymer dispersed liquid crystal as an external light feedback layer, J. Mater. Chem. C 3 (2015) 5566–5572.
[28] S. Kim, S. Ryu, Efficiency of flexible organic solar cells as a function of post-annealing temperatures, Curr. Appl. Phys. 10 (2010) e181–e184.
[29] S. Bertho, G. Janssen, T.J. Cleij, B. Conings, W. Moons, A. Gadisa, J. D'Haen, E. Goovaerts, L. Lutsen, J. Manca, Effect of temperature on the morphological and photovoltaic stability of bulk heterojunction polymer: fullerene solar cells, Sol. Energy Mater. Sol. Cells 92 (2008) 753–760.
[30] S.H. Chen, A.C. Su, H.L. Chou, K.Y. Peng, S.A. Chen, Phase behavior and molecular aggregation in bulk poly(2-methoxy-5-(2′-ethylhexyloxy)-1,4-phenylenevinylene), Macromolecules 37 (2004) 167–173.
[31] S.A. Jenekhe, J.A. Osaheni, Excimers and exciplexes of conjugated polymers, Science 265 (1994) 765–768.
[32] Y. Liu, X. Sun, H. Elim, W. Ji, Gain narrowing and random lasing from dye-doped polymer-dispersed liquid crystals with nanoscale liquid crystal droplets, Appl. Phys. Lett. 89 (2006) 011111–011113.
[33] E.M. Calzado, P.G. Boj, M.A. Díaz-García, Optimization of the laser properties of polymer films doped with N, N-Bis (3-methylphenyl)-N, N-diphenylbenzidine, Materials 2 (2009) 1288–1304.
[34] Z.E. Lampert, C.L. Reynolds Jr., J.M. Papanikolas, M.O. Aboelfotoh, Controlling morphology and chain aggregation in semiconducting conjugated polymers: the role of solvent on optical gain in MEH-PPV, J. Phys. Chem. B 116 (2012) 12835–12841.
[35] J. Wasey, A. Safonov, I. Samuel, W.L. Barnes, Efficiency of radiative emission from thin films of a light-emitting conjugated polymer, Phys. Rev. B 64 (2001) 205201.
[36] W. Holzer, A. Penzkofer, H. Tillmann, H.-H. Hörhold, Spectroscopic and travelling-wave lasing characterisation of Gilch-type and Horner-type MEH-PPV, Synth. Met. 140 (2004) 155–170.
[37] G. Samal, A. Tripathi, A. Biswas, S. Singh, Y. Mohapatra, Photoluminescence quantum efficiency (PLQE) and PL decay characteristics of polymeric light emitting materials, Synth. Met. 155 (2005) 344–348.
[38] M.D. McGehee, R. Gupta, S. Veenstra, E.K. Miller, M.A. Diaz-Garcia, A.J. Heeger, Amplified spontaneous emission from photopumped films of a conjugated polymer, Phys. Rev. B 58 (1998) 7035–7309.
[39] J. Ribierre, G. Tsiminis, S. Richardson, G. Turnbull, I. Samuel, H. Barcena, P. Burn, Amplified spontaneous emission and lasing properties of bisfluorene-cored dendrimers, Appl. Phys. Lett. 91 (2007) 081108.
[40] H.-C. Cheng, Y.-H. Huang, H.-W. Lin, C.-H. Chang, K.-T. Wong, C.-H. Kuan, C.-C. Wu, Continuously tunable organic solid-state DFB laser utilizing molecular reorientation in molecular glasses, Org. Electron 14 (2013) 2540–2545.
[41] W. Huang, L. Chen, L. Xuan, Efficient laser emission from organic semiconductor activated holographic polymer dispersed liquid crystal transmission gratings, RSC Adv. 4 (2014) 38606–38613.
[42] W. Huang, Y. Liu, L. Hu, Q. Mu, Z. Peng, C. Yang, L. Xuan, Second-order distributed feedback polymer laser based on holographic polymer dispersed liquid crystal grating, Org. Electron 14 (2013) 2299–2305.
[43] G. Turnbull, P. Andrew, W.L. Barnes, I. Samuel, Operating characteristics of a semiconducting polymer laser pumped by a microchip laser, Appl. Phys. Lett. 82 (2003) 313–315.
[44] E. Mele, A. Camposeo, R. Stabile, P. Del Carro, F. Di Benedetto, L. Persano, R. Cingolani, D. Pisignano, Polymeric distributed feedback lasers by room-temperature nanoimprint lithography, Appl. Phys. Lett. 89 (2006) 131109.
[45] H. Kogelnik, C. Shank, Coupled-wave theory of distributed feedback lasers, J. Appl. Phys. 43 (1972) 2327–2335.
[46] K. Okamoto, Fundamentals of Optical Waveguides, Academic press, Burlington, 2010.
[47] M. Tammer, A.P. Monkman, Measurement of the anisotropic refractive indices of spin cast thin poly (2-methoxy-5-(2′-ethyl-hexyloxy)-p-phenylenevinylene)(MEH–PPV) films, Adv. Mater 14 (2002) 210–212.